

## Authentication of NIFTI Neuroimages Using Lifting Wavelet Transform, Arnold Cat Map, Z-Transform, and Hessenberg Decomposition



Kamred Udham Singh<sup>1\*</sup>, Sun-Yuan Hsieh<sup>2</sup>, Chetan Swarup<sup>3</sup>, Teekam Singh<sup>4</sup>

<sup>1</sup> Department of Computer Science and Information Engineering, National Cheng Kung University, Tainan 701, Taiwan

<sup>2</sup> Department of Computer Science and Information Engineering, Institute of Medical Information, Institute of Manufacturing Information and Systems, Center for Innovative FinTech Business Models, and International Center for the Scientific Development of Shrimp Aquaculture, National Cheng Kung University, No. 1, University Road, Tainan 70101, Taiwan

<sup>3</sup> Department of Basic Science, College of Science and Theoretical Studies, Saudi Electronic University, Riyadh-Male Campus, 13316, Saudi Arabia

<sup>4</sup> School of Computer Science, University of Petroleum and Energy Studies, Dehradun 248007, India

Corresponding Author Email: [11004033@gs.ncku.edu.tw](mailto:11004033@gs.ncku.edu.tw)

<https://doi.org/10.18280/ts.390127>

### ABSTRACT

**Received:** 25 November 2021

**Accepted:** 12 January 2022

#### Keywords:

watermarking, NIFTI, lifting wavelet transform (LWT), image, Z-transform

The technological progress in digital medical imaging has enabled the diagnosis of various ailments, and thus upgraded the global healthcare system. In the era of coronavirus 2019 (COVID-19), telemedicine plays the crucial role of supporting remote medical consultation in rural locations. During the remote consultation, numerous medical images are sent to each radiologist via the Internet. There has been a surge in the number of attacks on digital medical images worldwide, which severely threatens authenticity and ownership. To mitigate the threat, this paper proposes a robust and secure watermarking approach for NIFTI images. Our approach painstakingly incorporates a watermark into the chosen NIFTI image slice, aiming to accurately fit the watermark, while preserving the medical information contained in the slice. Specifically, the original image was converted through the lifting wavelet transform (LWT), realizing excellent modification during insertion. Next, Z-transform was applied over the low-low (LL) band, and the Hessenberg decomposition (HD) was performed on the transformed band, which contains the maximum energy of the image. Afterwards, Arnold Cat map was employed to scramble the watermark, before inserting it into the slice. Simulation results show that our approach strikes a perfect balance between security, imperceptibility, and robustness against various attacks, as suggested by metrics like peak signal-to-noise ratio (PSNR), normalized correlation (NC), structural similarity index measure (SSIM), and universal image quality index Q.

## 1. INTRODUCTION

The recent improvements in digital communication and networking have significantly enhanced the capabilities of e-healthcare systems. For instance, the neuroimaging systems of modern hospitals are improved by the advancements in information and communication technology, e.g., the NIFTI medical images. Over the years, filmless, digital medical imaging has progressively replaced film-based medical imaging. The popularity of digital medical imaging, coupled with the development of telecommunications, facilitates qualified clinicians worldwide to communicate medical images and electronic patient data [1].

Medical image correction is vital to the accuracy of diagnosis and decision-making. Numerous supplementary technologies are required to correct medical images, including magnetic resonance imaging (MRI), computed tomography (CT) scan, and Color Doppler ultrasound. As diseases evolve, however, many diagnoses become insufficient, demanding teamwork amongst numerous experts to make an appropriate diagnosis [2]. In the healthcare industry, this teamwork is referred to as medical diagnostic assistance. Telemedicine plays a crucial role in various medical and healthcare

applications. One of the challenges to e-healthcare is to adhere to the authentication procedure of medical images, while sending these images over the Internet.

The primary difficulty in e-healthcare is to transmit data via the Internet, without sacrificing their ownership, privacy, and integrity against growing attacks [3]. Based on access control, various software solutions have been created to overcome the difficulty. Yet these solutions are inadequate to address the problem. Digital watermarking has been routinely utilized to authenticate medical image data, proving the data authenticity [4]. However, the watermarked images often still carry permanent anomalies, a cause for inaccurate diagnosis. According to medical professionals, permanent distortion of medical images is a severe issue with the transmission of digitally watermarked images. Some solutions have been developed to prevent persistent distortions.

Watermarking is often accomplished by carefully incorporating a brand or other significant information into the original image. Watermark embedding must be imperceptible to the human visual system, without degrading the image quality. Furthermore, the watermarking system must resist image processing attacks [5]. The watermarks must be recoverable, even if the image is intentionally exposed to

attacks like filtering and compression [6]. Once a medical information system is established, numerous watermarking techniques are often advised to protect medical images throughout regular transmission. These techniques fall into spatial and frequency domains [7]. In spatial-domain techniques, the pixel values of the original digital medical image are modified to directly embed watermarks. These techniques are well-established, and usually implemented with minimum computing load. In frequency-domain techniques, watermarks are often embedded into an altered image rather than the original image. Different transforms, namely, integer wavelet transform (IWT), discrete cosine transform (DCT), Curvelet transform, and discrete wavelet transform (DWT), are employed to convert the original image to the frequency domain. Compared with spatial-domain techniques, frequency-domain techniques are relatively durable, and capable of selecting pixels that resist specific types of image processing attacks [8].

The remaining of this paper is organized as follows: Section 2 presents the state-of-the-art image watermarking methods; Section 3 introduces the theorems and transforms used in our system; Section 4 talks about the proposed strategy of watermark insertion and extraction; Section 5 carries out simulations and evaluates the simulation results; Section 6 brings the intended research to a close.

## 2. LITERATURE REVIEW

Various watermarking schemes have been developed previously. For example, Hamidi et al. [9] proposed a DCT-based scheme, which includes a scrambled watermark bit in the middle-frequency band coefficients and relies on the Arnold transform to scramble the watermark. Multiple scholars [9-12] presented watermark encryption-based schemes, drawing on DCT or DWT. In addition, many other researchers [13-21] combined the DCT with DWT or singular value decomposition (SVD) into hybrid schemes and proved that the hybrid schemes are more robust than schemes based on a single transform.

Based on integer wavelet transform (IWT), Makbol and Khoo [22] designed a scheme with a higher robustness than watermark encryption-based schemes [9-11, 13-17]. IWT has a lower computational complexity. Jayashree & Bhuvaneshwaran [23] integrated Z transform and the bidiagonal SVD (BSVD) into a novel system: Starting with a three-level DWT, their system applies the Z transform to the selected high-low (HL) and high-high (HH) sub-bands, performs the BSVD on the Z transformed component, and embeds the singular values of a singular value matrix with the bits of an encrypted watermark. Despite its good imperceptibility, their system falls short in computing efficiency and robustness.

Inspired by discrete Curvelet transform (DCuT) and fast DCuT (FDCuT), Thanki et al. [19] developed a blind watermarking system for CT-scan, MRI, X-ray, and ultrasound images. Initially, the FDCuT was employed to deconstruct a medical image into several frequency coefficients. Then, the high-frequency curvelet coefficients were subjected to the DCT, and the mid-frequency band was selected for watermark insertion. Kunhu et al. [20] put forward a hybrid watermarking technique for X-ray images based on DWT, DCT, and SHA256-MD5: Firstly, each X-ray image was divided into regions of interest (ROIs) and non-ROIs (NROIs) using histogram image segmentation. Next, the

NROIs were partitioned into non-overlapping blocks and subjected to the DWT. After that, the DCT was applied to the low-low (LL) band, and the specified DCT coefficient was watermarked. The above two approaches [21, 22] are robust, but computationally complex.

Some watermarking algorithms have been developed based on matrix decomposition. Many academics resorted to the Hessenberg decomposition (HD) to construct watermarking systems in various ways. Su [24] created a watermarking technique based on the HD and the Arnold transform: The original image was separated into  $4 \times 4$  blocks, each of which was subjected to the HD. Then, the watermark was processed by the Arnold transform, and added into the Hessenberg orthogonal matrix. Abodena and Agoyi [25] suggested a color image watermarking system based on the DWT, fast Walsh Hadamard transform (FWHT), and HD: Firstly, the DWT was implemented on the red channel of the original image, then the FWHT. Following that, the FWHT coefficients were separated into blocks. In addition, the HD was applied to each block, and the watermark was inserted into the largest element of the first column of the H matrix. Their watermarking system can effectively withstand various attacks, such as scaling, blurring, filtering, JPEG2000, and noise addition. Liu et al. [26] designed a watermarking system that synthesizes the HD and DWT with SVD: During the embedding, the original image was divided into four sub-bands through multi-level DWT. The resulting coefficients were subjected to the HD. Afterwards, the SVD was applied to the watermark image. Finally, the watermark was embedded into the original image using the scale factor, which was determined through natural-inspired optimization. The watermarking system was found to strike a balance between robustness and invisibility, compared to earlier approaches under various attacks (e.g., noise addition, JPEG compression, filtering, and sharpening). Abduldaïm et al. [27] suggested a watermarking system based on the HD, DWT, and a logistic map: To begin with, the DWT was used to select the HL sub-band, and partition it into  $4 \times 4$  blocks. Each block was processed by a logistic map, allowing the block locations to be switched. Then, the watermark was incorporated into the H matrix by applying the HD to each block. Su and Chen [28] devised a new watermarking approach using the Arnold transform and the MD5 Hash algorithm: Firstly, the Arnold transform was performed on each color channel. Next, each channel was separated into  $4 \times 4$  blocks. The MD5 Hash algorithm was then called to select several blocks randomly, and the HD was implemented on each selected block. In the end, the watermark was inserted in the most prominent H matrix element of the HD, whose main advantage lies in the computing efficiency, compared to SVD and orthogonal-upper triangular matrix (QR) decomposition.

The literature survey shows that most watermarking approaches for medical images target the formats of .jpg, .png, .bmp, or DICOM [29]. There is no cutting-edge contribution for NIfTI images. Drawing on the previous results, this paper decides to develop a novel watermarking approach to authenticate NIfTI neuroimages by coupling the lifting wavelet transform (LWT), Arnold Cat map, Z-transform, and HD. The LWT and HD were adopted for their low computing complexity. Arnold Cat map is a simple way to scramble the watermark in image form before inserting it into an image, aiming to increase the security of the watermark. An unauthorized person cannot deduce anything from a watermark processed by Arnold Cat map. These three techniques were integrated in our approach to successfully

include the watermark into the original image, which eliminates a common risk of public watermarking algorithms: the intruder may do several Arnold transforms, and evaluate each version to see whether a visually relevant watermark is formed. Our approach makes three key contributions:

- Since the highest signal energy appears in the low-frequency sub-bands of a slice, watermark bits were added to this frequency sub-band to enhance the resilience of the watermarking system. The LWT and Z-transform were employed to improve security and robustness.
- The Hessenberg matrix of the HD was chosen for watermark embedding, in the light of the features of the human visual system, the similarity of pixels between the selected slice, and the varying importance of watermark bits.
- To ensure watermark security, the Arnold Cat map was adopted to jumble the watermark image. The proposed approach embeds the watermark in a specific slice of the original NifTI image, resulting in good watermark visibility, resilience, and security.

The simulation results of our approach were very promising: the mean peak signal-to-noise ratio (PSNR) was 55.34, and the structural similarity index measure (SSIM) was 0.9937. These results were better than the other existing schemes (Zermi et al. [3], Kunhu et al. [20], Zermi et al. [21], and Abodena & Agoyi [25]). The high robustness of our approach is evidenced by its outstanding performance against such attacks as average filtering, sharpening, motion blur and noise addition.

### 3. BACKGROUND

This section introduces the theorems and background utilized to design the proposed watermarking approach.

#### 3.1 LWT

The LWT was proposed by Wim Sweldens. The defining feature of the lifting technique is that all construction occurs in the spatial realm. With a low time-space complexity, the lifting technique outperforms traditional wavelet modifications, which generate high computing overheads. In fact, it is the most straightforward and efficient approach for computing wavelet transforms. Lifting transforms are independent of the Fourier transform.

Digital signals are generally composed of integer sequences. After wavelet processing, floating-point value sequences will be included in these signals, making it difficult to fully restore a digital signal. This calls for a transform method that retains the domain of the transformed signal. That is, the transform operator must be able to map an integer-based sequence signal back into another integer-based sequence signal. The domain of the transform is preserved in the LWT, which is always implemented in the integer-to-integer manner.

The LWT is widely used in image processing, thanks to its superior computing performance over traditional wavelet transforms. By the LWT, the original image is divided into four bands: LL, low-high (LH), HL, and HH. The low-frequency components of the LL band contain much more energy of the image than the high-frequency components of the other bands. Therefore, the LWT may be applied to the LL band repeatedly to split it into sub-bands. Following the lifting

technique, a signal can be constructed in three steps:

- **Split** – The given signal  $\omega(n)$  is split into non-overlapping odd  $\omega_o(n)$  and even  $\omega_e(n)$  sets:  $\omega_e(n) = \omega(2n)$ ,  $\omega_o(n) = \omega(2n + 1)$ .
- **Predict** – The odd set is predicted from the even set. Because the occurring polynomial components are compensated in the high pass, this step is also known as the high pass filtering phase. Mathematically, odd sets  $\omega_o(n)$  are predicted based on an even set  $\omega_e(n)$ , producing the difference  $\varphi(n) = \omega_o(n) - P_r[\omega_e(n)]$ , where,  $P_r[\cdot]$  is the predict operator;  $\varphi(n)$  is high-frequency component equaling the error between original set and the predicted value.
- **Update** – Using wavelet coefficient, the even set  $\omega_e(n)$  is updated to derive the scaling function. Because the moments in the low pass are also preserved, this step is sometimes called the low pass filtering phase. By applying an update operator  $U_p[\cdot]$ , the low-frequency component  $L(n)$  representing a coarse approximation of the original signal  $\omega(n)$  can be defined as  $L(n) = \omega_e(n) + U_p[\varphi(n)]$ .

#### 3.2 Z-transform

The Z-transform plays a significant role in discrete data processing. It provides an excellent tool for expressing, interpreting, and constructing discrete-time signals and systems [30]. Let  $\omega[m]$  be a discrete time signal. Then, the equivalent Z-transform can be described as:

$$\tau[z] = \sum_{i=-\infty}^{\infty} \omega[m]z^{-i} \quad (1)$$

where,  $z$  is the complex variable. When applied to a series of image pixels,  $\omega[m]$  may be greater than zero only in the range  $0 \leq i \leq \infty$ . Thus, formula (3) can be simplified into a one-sided Z-transform.

$$\tau[z] = \sum_{i=0}^{\infty} \omega[m]z^{-i} \quad (2)$$

To get the original signal  $\omega[m]$ , it is necessary to carry out the inverse Z-transform:

$$\omega[m] = Z^{-1}[\tau(z)] \quad (3)$$

where,  $\tau[z]$  is the Z-transform;  $Z^{-1}$  is the inverse Z-transform. Rabiner et al. numerically determined the Z-transform of a series of  $N$  samples [31]. Their approach, known as the chirp Z-transform, can compute the Z-transform efficiently as a circular contour at any arbitrary location in the  $z$ -plane. In digital image watermarking, their approach enhances the resilience and imperceptibility of the original image, and facilitates additional image processing tasks like filtering, interpolation, and correlation.

#### 3.3 HD

The HD [32] is a matrix factorization that decomposes a square matrix  $X$  based on orthogonal similarity:

$$X = Z * H * Z^T \quad (4)$$

Apply the Hessenberg decomposition on the matrix using the above Eq. (4).

$$S = \begin{bmatrix} 245 & 128 & 186 & 211 \\ 154 & 165 & 130 & 193 \\ 124 & 155 & 143 & 138 \\ 254 & 219 & 243 & 175 \end{bmatrix}$$

$$Z = \begin{bmatrix} 1.000 & 0 & 0 & 0 \\ 0 & -0.4784 & -0.5418 & -0.6911 \\ 0 & -0.3852 & -0.5777 & 0.7196 \\ 0 & -0.7891 & 0.6105 & 0.0677 \end{bmatrix}$$

$$H = \begin{bmatrix} 245.0000 & -299.3955 & -47.9847 & -59.6726 \\ -321.8820 & 491.6728 & 173.8680 & -25.9917 \\ 0 & 84.3554 & -20.3783 & 23.0342 \\ 0 & 0 & -37.7024 & 11.7054 \end{bmatrix}$$

$$Z^T = \begin{bmatrix} 1.000 & 0 & 0 & 0 \\ 0 & -0.4784 & -0.3852 & -0.7891 \\ 0 & -0.5418 & -0.5777 & 0.6105 \\ 0 & -0.6911 & 0.7196 & 0.0677 \end{bmatrix}$$

### 3.4 Arnold Cat map

Arnold Cat map randomly modifies the original positions of the pixels in the original medical image. This two-dimensional (2D) mapping technique has gained popularity in encryption and watermarking, owing to its simplicity, periodicity, and reversibility [9, 10]. The periodicity and reversibility imply that, if a transform is applied repeatedly to a given matrix, the starting data will be received after a full time. Arnold Cat map can be expressed as:

$$\begin{bmatrix} p' \\ q' \end{bmatrix} = \begin{bmatrix} 1 & l \\ m & lm + 1 \end{bmatrix} \begin{bmatrix} p \\ q \end{bmatrix} \text{mod } M \quad (5)$$

where,  $M$  is the size of the original image;  $p$  and  $q \in \{0, 1, 2, \dots, N - 1\}$  are control parameters that improve the security to determining the mapping frequency;  $\begin{bmatrix} p \\ q \end{bmatrix}$  is the pixel location in the image;  $\begin{bmatrix} p' \\ q' \end{bmatrix}$  is the pixel location after the transform.

Arnold Cat map only changes the image data, without affecting the intensity of the image. After multiple transforms, the link between neighboring pixels is thoroughly disrupted, and the image becomes twisted and nonsensical. In watermarking, Arnold Cat map is a pre-process to ensure security and minimize the likelihood of targeted attacks. In our approach, this transform is applied to the watermark logo image using a key (number of repetitions). Then, the transformed watermark is inserted to the original image. Apart from the security benefit, Arnold Cat map spreads the changes generated by watermark embedding with a significant gain factor in the whole image, making it aesthetically unrecognizable.

## 4. METHODOLOGY

This section firstly introduces the proposed hybrid watermark embedding approach, and then details the process of watermark extraction, as the reverse steps of watermark insertion.

### 4.1 Watermark embedding

Initially, the information of the original NifTI medical image is safely preserved. Then, a slice of NifTI image data is processed for watermarking. The watermark and the slice are both grayscale images. Through wavelet transform, the slice is divided into four frequency bands: LL, LH, HL, and HH. The vital data of the image is contained in the LL band, which is resistant to denoising attacks. Here, the Z-transform is applied on the LL band, and the transformed components are subjected to the HD. Meanwhile, the primary components of the watermark are processed by Arnold Cat map. After that, the altered watermark is inserted in the H matrix of the HD. The scaling factor (alpha) is used to control the watermark augmentation in the original data. The improved component is mixed with LL bands, and inversely transformed to recreate the original image. Finally, the watermarked medical image is combined with the electronic patient record (EPR) to obtain the watermarked NifTI image. The watermark embedding algorithm is detailed below:

Input: Size of the CT-Scan NifTI image I ( $630 \times 630$ )  
Size of grayscale watermark G ( $64 \times 64$ )

Output: Watermarked NifTI image

- Step 1. Extract patient metadata from the original NifTI image and select the slice N from the image.
- Step 2. Apply Arnold Cat map on the grayscale watermark using the key (formula (6)).

$$Z = ACM(G) \quad (6)$$

- Step 3. Perform two levels of LWT on the original image N to split it into four bands: LH, HL, LL, and HH.
- Step 4. Perform Z-transform on the LL band (formula (1)).

$$Z_{LL} = Z_{Transform}(LL) \quad (7)$$

- Step 5. Perform the HD on the LL band (formula (4)).

$$WHW^T = HD(Z_{LL}) \quad (8)$$

- Step 6. Embed the bits of the transformed watermark in the H matrix, and embed the watermark in the original image by:

$$H' = H + \delta Z \quad (9)$$

where,  $H$  is the factorized slice component of the original image;  $Z$  is the transformed watermark;  $\delta$  is the embedding strength.

- Step 7. Combine all the factorized components by:

$$F' = WH'W^T \quad (10)$$

- Step 8. Perform inverse Z-transform on  $F'$ :

$$K = Z_{inv}(F') \quad (11)$$

Step 9. Perform inverse IWT to obtain the final watermarked slice  $N'$ :

$$N' = ILWT(K) \quad (12)$$

Step 10. Embedded the patient metadata with a watermarked slice to obtain the final watermarked NifTI image.

#### 4.2 Watermark extraction

Watermark extraction is essential to any watermarking system. The original NifTI image is required to remove the watermark from the watermarked image. Here, the EPR is extracted from both the original and watermarked NifTI slices. Then, the LWT is applied to both slices, splitting each into four frequency bands: LL, LH, HL, and HH. Next, the Z-transform is implemented on these transformed components on the LL band, followed by the HD. The noisy components are extracted from the watermarked slice and subjected to Arnold Cat map to construct the watermarks. Our watermark extraction algorithm is detailed below.

**Input:** Original NifTI image and watermarked NifTI image

**Output:** Watermark X

**Step 1.** Extract patient information from both NifTI images I and  $I^+$ .

**Step 2.** Select the watermarked slices L and  $L^+$  from I and  $I^+$ .

**Step 3.** Decompose I and  $I^+$  through the LWT to obtain the LL band.

**Step 4.** Apply Z-transform on the LL band by:

$$Z_{LL} = Z_{Transform}(LL) \quad (13)$$

**Step 5.** Apply the HD on the  $Z_{LL}$  band by:

$$WHW^T = HD(Z_{LL}) \quad (14)$$

**Step 6.** Extract the watermark from the watermarked slice using the original slice of the NifTI image through the reverse process of the embedding approach:

$$X = (L^+ - L)/\delta \quad (15)$$

where,  $L^+$  is the watermarked slice of the NifTI image;  $X$  is the encrypted watermark component;  $L$  is the original slice of the NifTI image;  $\delta$  is the watermark embedding factor.

## 5. RESULTS AND DISCUSSION

Our watermarking approach was evaluated using the NifTI slice produced by a CT-Scan of a coronavirus 2019 (COVID19) patient obtained from <https://zenodo.org/record/3757476#.X0pwCnkzZPZ> [33] following ethical medical procedures, without disclosing the patient's name. The slice was used only for experimental purposes. The evaluation was carried out through simulation on MATLAB 2020b, using a computer operating on an 8-core Intel i7-11850H CPU (2.5GHz), Windows 10 computer, and 16GB RAM. Various NifTI images with a size of  $630 \times 630$  pixels and a .png watermark with a  $64 \times 64$  pixels resolution

and a bit depth of 8 bits.

### 5.1 Performance metrics

The imperceptibility of our watermarking approach was evaluated on six different NifTI images. The perceptibility of watermarks was measured by the PSNR:

$$MSE = \frac{1}{m * n} \sum_{i=0}^m \sum_{j=0}^n (A_{ij} - B_{ij})^2 \quad (16)$$

$$PSNR = 10 * \log_{10} \frac{(Max)^2}{\frac{1}{m * n} \sum_{i=0}^m \sum_{j=0}^n (A_{ij} - B_{ij})^2} \quad (17)$$

$$SNR = 10 * \log_{10} \frac{\sum_{i=1}^n \sum_{j=1}^m (A_{ij})^2}{\sum_{i=1}^n \sum_{j=1}^m (A_{ij} - B_{ij})^2} \quad (18)$$

The robustness of our approach was estimated by normalized correlation (NC), the difference between the original slice of the NifTI image I and the watermarked slice of the NifTI image  $I^+$  [7]:

$$NC = \frac{\sum_{x=1}^M \sum_{y=1}^N w(x, y) \times w^*(x, y)}{\sum_{x=1}^M \sum_{y=1}^N w^2(x, y)} \quad (19)$$

The universal image quality index Q [32] was defined as:

$$Q = \frac{4\sigma_{xy}\bar{x}\bar{y}}{(\sigma_x^2 + \sigma_y^2)[(\bar{x})^2 + (\bar{y})^2]} \quad (20)$$

The SSIM was adopted to assess the similarity between the original and watermark images. The SSIM value ranges from -1 to +1; if SSIM=1, the original and watermark images are identical. The SSIM can be calculated by:

$$SSIM(x, y) = \frac{(2\mu_x\mu_y + c_1)(2\sigma_{xy} + c_2)}{(\mu_x^2 + \mu_y^2 + c_1)(\sigma_x^2 + \sigma_y^2 + c_2)} \quad (21)$$

where,  $\mu_x$  and  $\mu_y$  are the mean values of the original image and the watermarked image, respectively;  $\sigma_x^2$  and  $\sigma_y^2$  are the variances of the original image and the watermarked image, respectively;  $\sigma_{xy}$  is the covariance;  $c_1$  and  $c_2$  are free parameters.

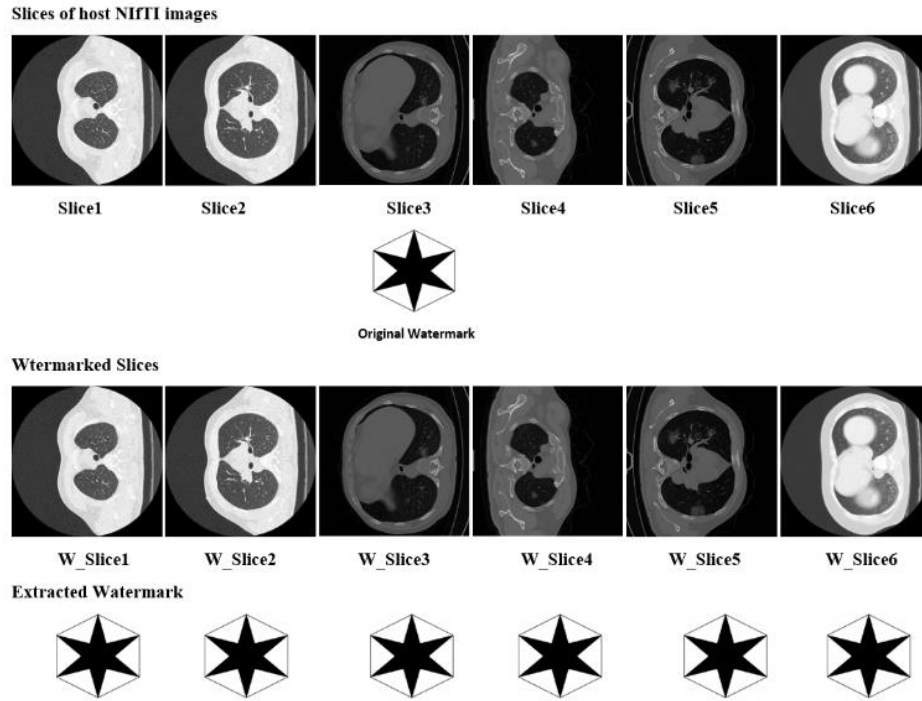
### 5.2 Results and analysis

The imperceptibility and robustness of our approach were verified on six different NifTI images: Slice 1, Slice 2, Slice 3, Slice 4, Slice 5, and Slice 6. The slice size was set to  $630 \times 630$ , and the watermark size to  $64 \times 64$ . Figure 1 reports the simulation results, and Figure 2 displays the graphical representation of the relevant parameters. The watermarked NifTI images retain the metadata encoding the details of the COVID-19 impacted individuals.

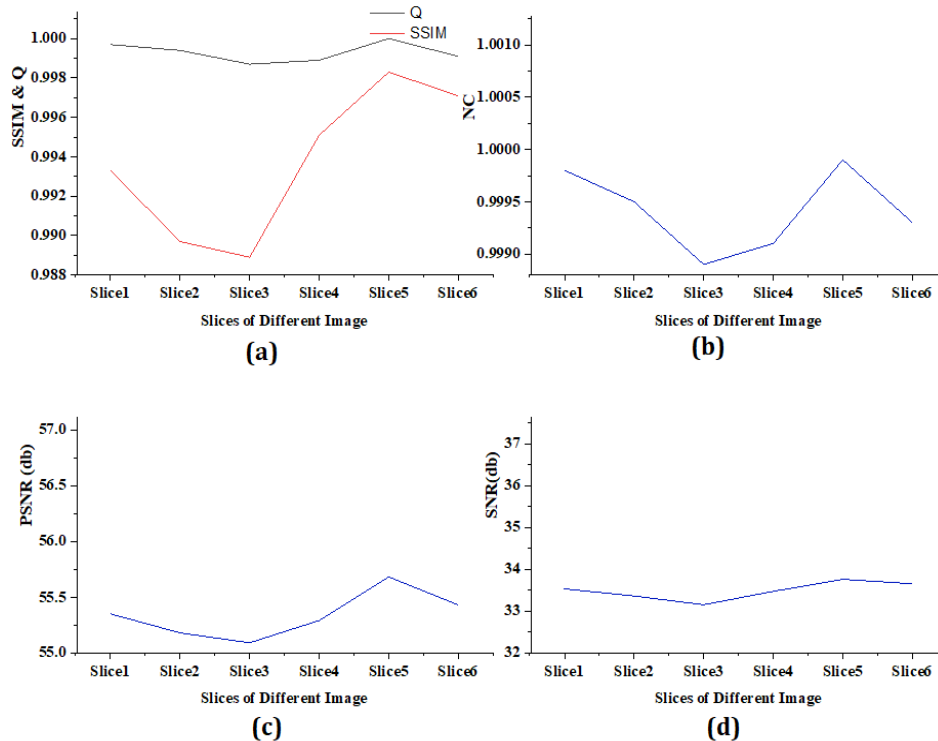
The performance of our approach was tested using each slice of the six images. The watermarked slices and the evaluation parameters are shown in Table 1. The image quality metrics NC, SSIM, and Q were all close to one, suggesting a nearly perfect correlation between the original and watermarked images. The PSNR of the watermarked image was greater than 52 dB, a sign of exceptionally high quality

for the watermarked image. Tables 2 and 3 compare the results of our approach with those of other existing methods. The comparison shows that our approach achieved more significant results than those methods. As shown in Table 2, our approach realized better PSNR than the contrastive methods, though schemes like Zermi et al. [3], Thanki et al. [21], Kunhu et al. [20], Zermi et al. [21] also saw good PSNRs. As shown in Table 3, the SSIM of our approach was closer to one than that of any other method, indicating that the superior quality of the watermarks generated by our approach.

Medical practitioners or radiologists must ensure that the perfect medical image is diagnosed after successfully extracting the watermark from the given NIFTI image. This is a matter of life or death to the patient. A watermark may be a logo or an image containing the unique patient information, such as patient ID and patient name. Consequently, our approach may play an essential role in verifying NifTI images, laying a solid basis for correct diagnoses of epidemics like COVID-19.



**Figure 1.** Slices of original NifTI images, watermark images and extracted watermarks



**Figure 2.** (a) SSIM and Q of the watermarked slices, (b) NC of the watermarked slices, (c) PSNR of the watermarked slices, (d) PSNR of the watermarked slices

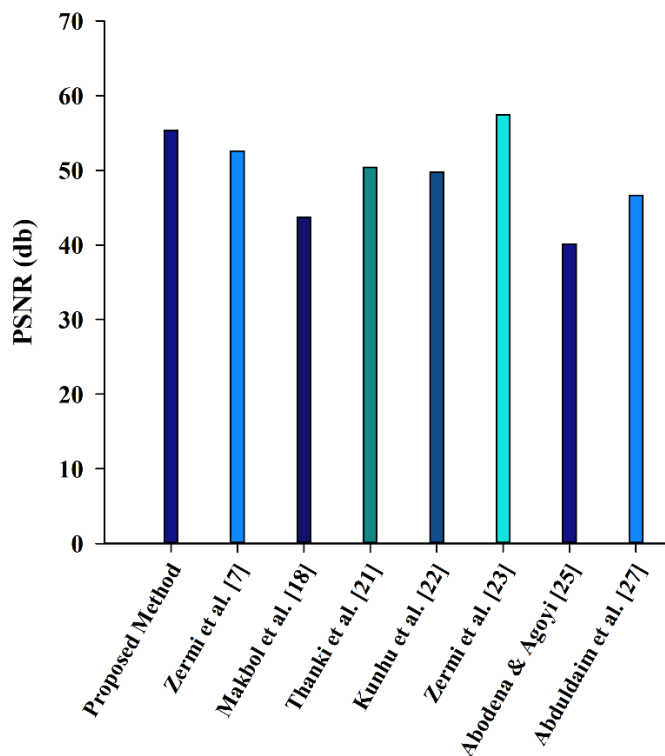
**Table 1.** Qualitative analysis on the watermarked slices of the images

Medical Images	NC	Q	PSNR	SNR	SSIM
Slice1	0.9997	0.9998	55.35	33.53	0.9933
Slice2	0.9994	0.9995	55.18	33.36	0.9897
Slice3	0.9987	0.9989	55.09	33.15	0.9889
Slice4	0.9989	0.9991	55.29	33.47	0.9951
Slice5	1	0.9999	55.68	33.76	0.9983
Slice6	0.9991	0.9993	55.43	33.65	0.9971

Table 2 compares the PSNR of our approach with that of the other existing methods (Zermi et al. [3], Makbol and Khoo [22], Thanki et al. [21], Kunhu et al. [20], Zermi et al. [21], Abodena & Agoyi [25], and Abduldaïm et al. [27]) on six different NIfTI images. It can be observed that the PSNR of our approach appeared between 55.09dB and 55.68dB, while

**Table 2.** Comparison of PSNR

Proposed Method	Zermi et al. [3]	Makbol and Khoo [22]	Thanki et al. [19]	Kunhu et al. [20]	Zermi et al. [21]	Abodena & Agoyi [25]	Abduldaïm et al. [27]
55.35	55.85	43.67	55.06	45.83	57.41	40.15	49.90
55.18	57.04		50.27	41.18		40.13	42.74
55.09	44.91		48.99	46.93		40.15	47.10
55.29			47.18	64.93		40.15	46.80
55.68							
55.43							
<b>55.34</b>	<b>52.60</b>	<b>43.67</b>	<b>50.38</b>	<b>49.78</b>	<b>57.41</b>	<b>40.15</b>	<b>46.64</b>



**Figure 3.** Comparison of mean PSNR

Table 3 compares the SSIM of our approach and that of the other methods: Zermi et al. [3], Kunhu et al. [20], Zermi et al. [23], and Abodena & Agoyi [25]. The mean SSIMs of Zermi et al. [3], Kunhu et al. [20], Zermi et al. [23], and Abodena & Agoyi [25] were 0.9985, 0.9957, 0.9998, and 1, respectively, while that of our approach was 0.9937. Thus, the SSIM of our

that of the other methods fell in 40.13-64.93dB: 44.91-57.04dB for Zermi et al. [3]; 43.67dB for Makbol and Khoo [22]; 47.18-55.06dB for Thanki et al. [19]; 41.18-64.93dB for Kunhu et al. [20]; 57.41dB for Zermi et al. [21]; 40.13-40.159dB for Abodena & Agoyi [25]; 42.74-49.90dB for Abduldaïm et al. [27]. The mean PSNRs of our approach, Zermi et al. [3], Makbol and Khoo [22], Thanki et al. [19], Kunhu et al. [20], Zermi et al. [21], Abodena & Agoyi [25], and Abduldaïm et al. [27] were 52.60dB, 43.67dB, 50.38dB, 49.78dB, 57.41dB, 40.15dB and 46.64dB, respectively. Overall, the PSNR of our approach was more significant than the other methods. Of course, Zermi et al. [3], Thanki et al. [21], Kunhu et al. [20], Zermi et al. [21] had fairly good PSNRs. This means our approach has an extraordinarily sound imperceptibility. Figure 3 compares the mean PSNRs between our approach and the other methods.

approach was closer to one than that of any other method. This means our approach can fully guarantee watermarking quality.

**Table 3.** Comparison of SSIM

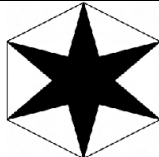
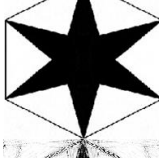
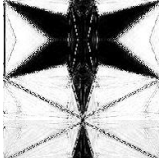
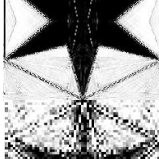

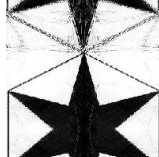
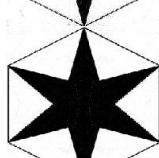
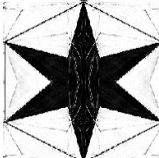
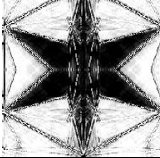
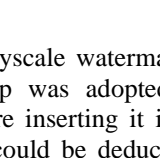
Proposed Method	Zermi et al. [3]	Kunhu et al. [20]	Zermi et al. [21]	Abodena & Agoyi [25]
0.9933	.9997	.9933	0.9998	1.000
0.9897	.9998	.9893		1.000
0.9889	.9961	.9988		1.000
0.9951		.9998		1.000
0.9983		.9934		
0.9971		1.000		
		<b>Avg SSIM</b>		
<b>0.9937</b>	<b>.9985</b>	<b>.9957</b>	<b>0.9998</b>	<b>1</b>

### 5.3 Robustness analysis

The above results show that our approach can achieve significant results on different slices of various NIfTI images. Here, the robustness of our approach is evaluated against different image processing attacks. The watermarked images were attacked by the addition of the following noises: salt-and-pepper noise, Gaussian noise, Poisson noise, compression noise, speckle noise, etc. The watermarks extracted from the tampered images are presented in Table 4. The results show that our approach was robust against these various attacks, and outshined Zermi et al. [3], Makbol and Khoo [22], Abodena & Agoyi [25], and Abduldaïm et al. [27]. The quality of the extracted watermarks was decreased yet acceptable under certain attacks. The robustness of our approach is inversely related to the watermark quality. Nevertheless, a trade-off must be considered between watermark quality and robustness [24].



**Table 4.** Watermarks extracted under various attacks

Name of Attack	PSNR of the Slice after the attack	SSIM of the Slice after the attack	Extracted Watermark	NC of Extracted Watermark
Salt and pepper noise (.003)	33.54	.9245		.9531
Speckle noise (.004)	38.47	.9653		.9764
Gaussian low-pass filter (3X3)	33.41	.8546		.9612
Median (3X3)	32.54	.8356		.9685
Histogram equalization	21.35	.8757		.9284
Average filter (3X3)	31.89	.8382		.9657
Gaussian noise (.005)	30.64	.6854		.9336
JPEG 80 compression	33.95	.8354		.9661
Sharpening (0.2)	34.18	.9399		.9456
Motion blur (0.2)	26.48	.7385		.8528

## 6. CONCLUSIONS

This paper presents a novel watermarking approach for NIfTI images, drawing on the LWT, Z-transform, HD, and Arnold Cat map. To verify its robustness, the approach was simulated on multiple NIfTI slices (512×512) from a CT-scan,

as well as a grayscale watermark (64×64). Specifically, the Arnold Cat map was adopted to transform the encoded watermark before inserting it into the original image. As a result, nothing could be deduced, even if the watermark is extracted by an unauthorized person. This eliminates a common risk of public watermarking algorithms: the intruder



may do several Arnold transforms and evaluate each version to see whether a visually relevant watermark is formed. Next, the altered watermark was entered into the Hessenberg matrix. Simulation results show that our approach outperformed prior comparable systems in terms of invisibility, durability, and capacity. To authenticate NIFTI images, our approach selects a random slice out of the multiple slices of the original NIFTI image. Each slice of the image may be authenticated by our approach, in order to insert a watermark in more than one or all image slices. Consequently, our watermarking approach can be used to authenticate and identify the appropriate NIFTI medical image for diagnosing CT-scan and MRI images. The limitation of our approach is that: if someone scrambles the slices of the NIFTI image, it would be challenging to identify the watermarked file. In this case, every slice must be checked for watermark extraction, which is a time-consuming task. This problem will be dealt with in future research.

## REFERENCES

- [1] Boussif, M., Aloui, N., Cherif, A. (2020). DICOM imaging watermarking for hiding medical reports. *Medical & Biological Engineering & Computing*, 58(11): 2905-2918. <https://doi.org/10.1007/s11517-020-02269-8>
- [2] Bastani, A., Ahouz, F. (2020). High capacity and secure watermarking for medical images using Tchebichef moments. *Radioengineering*, 29(4): 636-643. <https://doi.org/10.13164/re.2020.0636>
- [3] Zermi, N., Khaldi, A., Kafi, M.R., Kahlessenane, F., Euschi, S. (2021). Robust SVD-based schemes for medical image watermarking. *Microprocessors and Microsystems*, 84: 104134. <https://doi.org/10.1016/j.micpro.2021.104134>
- [4] Singh, K.U., Singh, V.K., Singhal, A. (2018). Color image watermarking scheme based on QR factorization and DWT with compatibility analysis on different wavelet filters. *Journal of Advanced Research in Dynamical and Control Systems*, 10(6): 1796-1811.
- [5] Araghi, T.K., Abd Manaf, A. (2019). An enhanced hybrid image watermarking scheme for security of medical and non-medical images based on DWT and 2-D SVD. *Future Generation Computer Systems*, 101: 1223-1246. <https://doi.org/10.1016/j.future.2019.07.064>
- [6] Ustubioglu, A., Ulutas, G., Ustubioglu, B. (2019). IWT-MDE based reversible thermal image watermarking enhanced with secret sharing mechanism. *Multimedia Tools and Applications*, 78(16): 22269-22299. <https://doi.org/10.1007/s11042-019-7529-0>
- [7] Hu, H.T., Hsu, L.Y., Chou, H.H. (2020). An improved SVD-based blind color image watermarking algorithm with mixed modulation incorporated. *Information Sciences*, 519: 161-182. <https://doi.org/10.1016/j.ins.2020.01.019>
- [8] Singh, K.U., Singhal, A. (2018). Channelized noise augmentation to endorse DICOM medical image for diagnosing. *Journal of Advanced Research in Dynamical and Control Systems*, 10(6): 2228-2247.
- [9] Hamidi, M., El Haziti, M., Cherifi, H., El Hassouni, M. (2018). Hybrid blind robust image watermarking technique based on DFT-DCT and Arnold transform. *Multimedia Tools and Applications*, 77(20): 27181-27214. <https://doi.org/10.1007/s11042-018-5913-9>
- [10] Khare, P., Srivastava, V.K. (2019). Secure and robust image watermarking scheme using homomorphic transform, SVD and Arnold transform in RDWT domain. *Advances in Electrical and Electronic Engineering*, 17(3): 343-351. <https://doi.org/10.15598/aeec.v17i3.3154>
- [11] Sun, L., Xu, J., Liu, S., Zhang, S., Li, Y., Shen, C.A. (2018). A robust image watermarking scheme using Arnold transform and BP neural network. *Neural Computing and Applications*, 30(8): 2425-2440. <https://doi.org/10.1007/s00521-016-2788-4>
- [12] Singh, D., Singh, S.K. (2017). DWT-SVD and DCT based robust and blind watermarking scheme for copyright protection. *Multimedia Tools and Applications*, 76(11): 13001-13024. <https://doi.org/10.1007/s11042-016-3706-6>
- [13] Chang, C., Shen, J. (2017). Features classification forest: a novel development that is adaptable to robust blind watermarking techniques. *IEEE Trans Image Process* 26(8): 3921-3935. <https://doi.org/10.1109/TIP.2017.2706502>
- [14] Singh, S., Bhatnagar, G. (2018). A new robust watermarking system in integer DCT domain. *Journal of Visual Communication and Image Representation*, 53: 86-101. <https://doi.org/10.1016/j.jvcir.2018.03.006>
- [15] Kang, X.B., Zhao, F., Lin, G.F., Chen, Y.J. (2018). A novel hybrid of DCT and SVD in DWT domain for robust and invisible blind image watermarking with optimal embedding strength. *Multimedia Tools and Applications*, 77(11): 13197-13224. <https://doi.org/10.1007/s11042-017-4941-1>
- [16] Hsu, L., Hu, H. (2017). Robust blind image watermarking using crisscross inter-block prediction in the DCT domain. *Journal of Visual Communication and Image Representation*, 46: 33-47. <https://doi.org/10.1016/j.jvcir.2017.03.009>
- [17] Zhou, N.R., Hou, W.M.X., Wen, R.H., Zou, W.P. (2018). Imperceptible digital watermarking scheme in multiple transform domains. *Multimedia Tools and Applications*, 77(23): 30251-30267. <https://doi.org/10.1007/s11042-018-6128-9>
- [18] Assini, A., Badri, A., Safi, K., Sahel, A., Baghdad, A. (2018). A robust hybrid watermarking technique for securing medical image. *International Journal of Intelligent Engineering & Systems*, 11(3): 169-176. <https://doi.org/10.22266/ijies2018.0630.18>
- [19] Thanki, R., Borra, S., Dwivedi, V., Borisagar, K. (2017). An efficient medical image watermarking scheme based on FDCuT-DCT. *Engineering Science and Technology, an International Journal*, 20(4): 1366-1379. <https://doi.org/10.1016/j.jestch.2017.06.001>
- [20] Kunhu, A., Al-Ahmad, H., Taher, F. (2017). Medical images protection and authentication using hybrid DWT-DCT and SHA256-MD5 hash functions. 2017 24th IEEE International Conference on Electronics, Circuits and Systems (ICECS), pp. 397-400. <https://doi.org/10.1109/ICECS.2017.8292084>
- [21] Zermi, N., Khaldi, A., Kafi, R., Kahlessenane, F., Euschi, S. (2021). A DWT-SVD based robust digital watermarking for medical image security. *Forensic Science International*, 320: 110691. <https://doi.org/10.1016/j.forsciint.2021.110691>
- [22] Makbol, N.M., Khoo, B.E. (2014). A new robust and secure digital image watermarking scheme based on the integer wavelet transform and singular value decomposition. *Digital Signal Processing*, 33: 134-147.

- <https://doi.org/10.1016/j.dsp.2014.06.012>
- [23] Jayashree, N., Bhuvaneshwaran, R.S. (2019). A robust image watermarking using Z-transform, discrete wavelet transform and bidiagonal singular value decomposition. *Tech Science Press*, 58(1): 263-285. <https://doi.org/10.32604/cmc.2019.03924>
- [24] Su, Q. (2016). Novel blind colour image watermarking technique using Hessenberg decomposition. *IET Image Processing*, 10(11): 817-829. <https://doi.org/10.1049/iet-ivr.2016.0048>
- [25] Abodena, O., Agoyi, M. (2018). Color image blind watermarking scheme based on fast Walsh Hadamard transform and Hessenberg decomposition. *J. Studies in Informatics and Control*, 27(3): 339-348. <https://doi.org/10.24846/v27i3y201809>
- [26] Liu, J., Huang, J., Luo, Y., Cao, L., Yang, S., Wei, D., Zhou, R. (2019). An optimized image watermarking method based on HD and SVD in DWT domain. *IEEE Access*, 7: 80849-80860. <https://doi.org/10.1109/ACCESS.2019.2915596>
- [27] Abduldaim, A.M., Waleed, J., Mazher, A.N. (2020). An efficient scheme of digital image watermarking based on Hessenberg factorization and DWT. *IEEE International Conference on Computer Science and Software Engineering*, pp. 180-185. <https://doi.org/10.1109/CSASE48920.2020.9142096>
- [28] Su, Q., Chen, B. (2017). A novel blind color image watermarking using upper Hessenberg matrix. *AEU-International Journal of Electronics and Communications*, 78: 64-71. <https://doi.org/10.1016/j.aeue.2017.05.025>
- [29] Singh, K.U., Abu-Hamatta, H.S., Kumar, A., Singhal, A., Rashid, M., Bashir, A.K. (2022). Secure watermarking scheme for color DICOM images in telemedicine applications. *CMC-Computers, Materials & Continua*, 70(2): 2525-2542. <https://doi.org/10.32604/cmc.2022.019302>
- [30] Ho, A.T., Zhu, X., Shen, J., Marziliano, P. (2008). Fragile watermarking based on encoding of the zeroes of the z-transform. *IEEE Transactions on Information Forensics and Security*, 3(3): 567-569. <https://doi.org/10.1109/TIFS.2008.926994>
- [31] Rabiner, L.R., Schafer, R.W., Rader, C.M. (1969). The chirp z-transform algorithm and its application. *Bell System Technical Journal*, 48(5): 1249-1292. <https://doi.org/10.1002/j.1538-7305.1969.tb04268.x>
- [32] Golub, G.H., Loan, C.F.V. (1996). *Matrix Computations*. Baltimore: Johns Hopkins University Press.
- [33] Ma, J., Ge, C., Wang, Y., et al. (2020). COVID-19 CT Lung and Infection Segmentation Dataset [Data set]. Zenodo. <https://doi.org/10.5281/zenodo.3757476>